Inorganic Chemistry

pubs.acs.org/IC Article

$LaHg_3Mn_4O_{12}$: An A-Site Nonmagnetic Quadruple Perovskite Oxide with Enhanced Half-Metallic Performances

Maocai Pi,* Ilya Semenov, Evgenia Komleva, Xi Shen, Huifen Ren, Zhehong Liu, Jie Zhang, Shuai Tang, Xubin Ye, Zhiwei Hu, Chang-Yang Kuo, Chien-Te Chen, Zhao Pan, Yao Shen, Richeng Yu, Sergey V. Streltsov,* and Youwen Long*

Cite This: *Inorg. Chem.* 2026, 65, 7451−7458 Read Online

ACCESS | Metrics & More | Article Recommendations

ABSTRACT: An A-site-ordered $AA'_3B_4O_{12}$-type quadruple perovskite oxide $LaHg_3Mn_4O_{12}$ was prepared by using high-pressure and high-temperature methods. The compound crystallizes in cubic $Im\bar{3}$ symmetry with a lattice parameter a = 7.5949(2) Å. The introduction of Hg^{2+} at the A′ site leads to a significant increase in the Mn−O−Mn bond angle, up to 159.5°. A ferromagnetic phase transition is found to occur at the Curie temperature: $T_C \approx 280$ K, accompanied by a large saturation magnetic moment of 13.0 μ_B/f.u. A corresponding anomaly in the electrical resistivity is observed near T_C. First-principles calculations reveal a half-metallic electronic band structure with a wide minority-spin energy gap of ∼2.0 eV, while the majority-spin states contribute to metallic electrical transport. The current sample, $LaHg_3Mn_4O_{12}$ thus provides the first example of A'-site nonmagnetic quadruple perovskite oxide with half-metallic behavior. Moreover, compared with other isostructural $RCu_3Mn_4O_{12}$ (R = rare earth and Bi) half-metals with magnetic Cu^{2+} at the A' site, $LaHg_3Mn_4O_{12}$ exhibits significant enhancement in both the minority-spin energy gap and saturation magnetization, making it promising for potential spintronic applications.

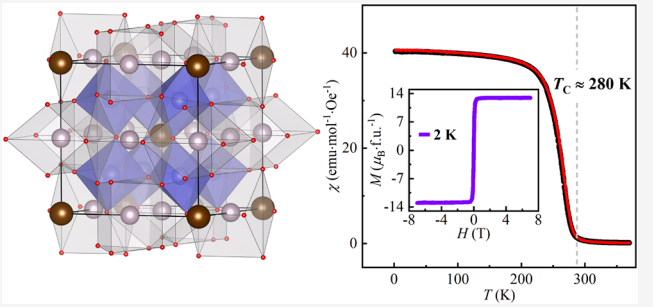

1. INTRODUCTION

A-site-ordered quadruple perovskite oxides with the chemical formula $AA'_3B_4O_{12}$ show many interesting physical properties, since both A′ and B sites can accommodate transition metals with intersite and/or intrasite electronic interactions. For example, a giant dielectric constant is reported in $CaCu_3Ti_4O_{12}$,[1−3] spin-driven multiferroicity and topological magnetoelectricity are found to occur in La/Bi/$TbMn_3Cr_4O_{12}$,[4−6] heavy Fermion behavior is observed in $CaCu_3Ru_4O_{12}$,[7,8] and charge transfer and charge disproportionation are observed in $RCu_3Fe_4O_{12}$ (R = rare earth and Bi).[9−11] Most $AA'_3B_4O_{12}$ perovskites have a cubic $Im\bar{3}$ symmetry. In this structure, the strong Jahn−Teller magnetic ions like Cu^{2+} and Mn^{3+} usually occupy the A′ site, forming square-coordination $A'O_4$ units, which connect with the BO_6 octahedra by corner-sharing O atoms. The presence of A′-site magnetic ions with smaller size leads to heavy tilting of BO_6 octahedra, so that the typical B−O−B bond angle is reduced to about 140°.[12]

$RCu_3Mn_4O_{12}$ quadruple perovskite oxides have been widely studied due to their high ferrimagnetic order temperatures, as well as their half-metallic electronic properties with completely spin-polarized carriers in principle.[13−16] However, since the A′-site Cu contributes to the band structure near the Fermi level, a reduced minority-spin half-metallic energy gap (typically only about 0.3 eV) emerges.[15,17,18] Such a narrow gap is prone to spin-flip scattering caused by thermal excitation at finite temperatures, and thereby severely suppresses the spin polarization rate. In addition, the Cu ions at the A′ site are antiferromagnetically coupled with the Mn ions at the B site in $RCu_3Mn_4O_{12}$, which greatly decreases the net magnetic moment.[19,20] Therefore, it is highly desirable to enhance the half-metallic band gap and the total spin moment as well for possible applications of these Mn-based quadruple perovskite half-metals.

In perovskite oxides, the ionic size and electronic configuration of the constituent cations play a crucial role in determining the magnetic and electrical properties.[21,22] If Cu^{2+} can be replaced by a larger-sized and nonmagnetic cation in $RCu_3Mn_4O_{12}$, the spin interactions and electronic band structure will be changed significantly. It is thus possible to

Received: January 28, 2026
Revised: March 16, 2026
Accepted: March 23, 2026
Published: March 25, 2026

https://doi.org/10.1021/acs.inorgchem.6c00539
Inorg. Chem. 2026, 65, 7451−7458

enhance the half-metallic band gap as well as the total spin moment simultaneously. In this paper, by using a larger-sized nonmagnetic Hg^{2+} to replace the magnetic Cu^{2+} at the A′ site, a novel A-site ordered quadruple perovskite oxide $LaHg_3Mn_4O_{12}$ was synthesized. Different from the ferrimagnetic $RCu_3Mn_4O_{12}$, $LaHg_3Mn_4O_{12}$ shows ferromagnetic (FM) ordering near room temperature with a considerably enhanced saturation magnetization up to 13.0 μ_B/f.u. Moreover, the minority-spin half-metallic gap substantially increases to 2.0 eV, making $LaHg_3Mn_4O_{12}$ a promising half-metal for potential applications in advanced spintronic devices.

2. EXPERIMENTAL AND COMPUTATIONAL METHODS

Highly pure (≥99.9%) La_2O_3, HgO, Mn_2O_3 and MnO_2 powders were mixed in a 1:6:1:6 mol ratio and ground thoroughly in an agate mortar within an argon-filled glovebox. The La_2O_3 powder was presintered at 1373 K for 24 h to remove any adsorbed H_2O and CO_2. Then the mixture was sealed into a platinum capsule 2 mm in diameter and 4 mm in height and treated at 15 GPa and 1373 K for 20 min in a Walker-type two-stage high-pressure apparatus. Once the heating time was finished, the sample was quenched to room temperature and the pressure was slowly released to ambient pressure within 15 h. It is worth noting that high-pressure and high-temperature conditions are necessary to synthesize $LaHg_3Mn_4O_{12}$. Conventional ambient-pressure solid-state reactions failed completely due to Hg volatilization, while attempts at 9 GPa and high temperatures still yielded considerable impurity phases. We thus believe that a pressure well above 10 GPa is essential to prepare high-quality $LaHg_3Mn_4O_{12}$, as reported for the synthesis of other Hg-included perovskite oxides.[23−25] The room-temperature synchrotron powder X-ray diffraction (SXRD) pattern at a wavelength of 0.420 Å was collected using a large Debye−Scherrer camera installed at the BL02B2 beamline of SPring-8. The Rietveld refinement for the SXRD data was performed using the GSAS program.[26] The selected area electron diffraction (SAED) was performed at room temperature by using a JEOL ARM200F transmission electron microscope equipped with double Cs correctors for the condenser and objective lens along the [001], [110], and [111] zone axes, respectively. The soft X-ray absorption spectroscopy (XAS) measurements were performed in total electron yield mode at the TLS11A beamline of the National Synchrotron Radiation Research Center in Taiwan. The magnetic susceptibility and magnetization were measured with a superconducting quantum interference device (SQUID) magnetometer (Quantum Design, MPMS 3). The specific heat data and the resistivity and magnetoresistance measurements, were collected by using a physical property measurement system (Quantum Design, PPMS-9T).

The projector augment-wave (PAW) implementation of the Vienna ab initio simulation package (VASP)[27] using the GGA+U method in the rotationally invariant form,[28] was used with Perdew−Burke−Ernzerhof version of the exchange-correlation functional.[29] The cutoff energy for the plane-wave basis set was 500 eV. For all the calculations, a 4 × 4 × 4 k-point mesh was chosen. It has previously been shown that the choice of the U value can affect the ground magnetic state of the parent compound.[30] Therefore, the effective Hubbard parameter U was taken to be 3.0 and 4.5 eV, and Hund's parameter J_H was chosen as 1.0 eV.

3. RESULTS AND DISCUSSION

Figure 1a displays the SXRD pattern of $LaHg_3Mn_4O_{12}$ measured at room temperature. All diffraction peaks can be successfully indexed to the cubic $Im\bar{3}$ (No. 204) space group. The superlattice reflections (111) and (130) are clearly visible in the pattern, which are characteristic features of A-site ordering in quadruple perovskites. Further evidence for the ordering is provided by the SAED pattern along the [001] direction [inset of Figure 1a], where pronounced (110) and (130) diffraction spots are observed. In $Im\bar{3}$ symmetry, La and Hg are arranged in a 1:3 order at the specific Wyckoff positions 2a (0, 0, 0) and 6b (0, 0.5, 0.5), respectively. The Mn atoms at the B-site occupy the 8c (0.25, 0.25, 0.25) Wyckoff site, while the O atoms are located at the 24g (0, y, z) site. The SXRD pattern of $LaHg_3Mn_4O_{12}$ can be well-fitted based on the

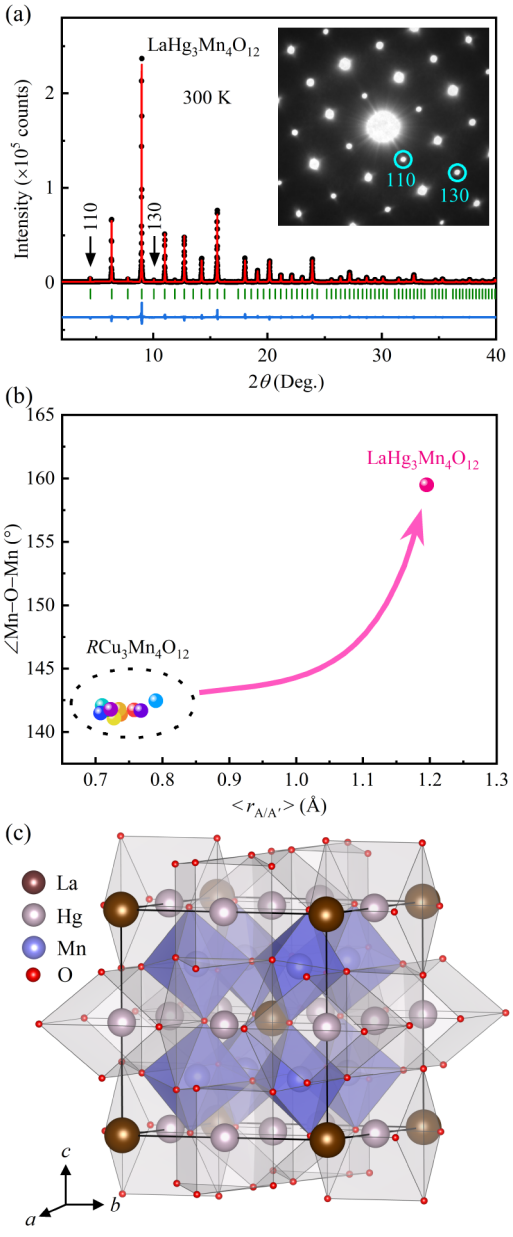

Figure 1. (a) SXRD and refined patterns of $LaHg_3Mn_4O_{12}$ at room temperature with the space group $Im\bar{3}$. The observed (black dot), calculated (red line), and difference (blue line) profiles are shown. The green ticks indicate the nuclear peaks. The peaks pointed out by the black arrows correspond to the (110) and (130) reflections, which are signatures of the A-site-ordered quadruple perovskite structure. The inset shows the SAED pattern along the [100] zone axis. The diffraction spots highlighted by the blue lines correspond to the (110) and (130) reflections. (b) ∠Mn−O−Mn as a function of the average A/A′-site ionic radius $< r_{A/A'} >$ for $LaHg_3Mn_4O_{12}$ and $RCu_3Mn_4O_{12}$. (c) Crystal structure of $LaHg_3Mn_4O_{12}$. The B-site MnO_6 octahedra and A′-site HgO_8 units connect with each other by corner-sharing of the O atoms.

https://doi.org/10.1021/acs.inorgchem.6c00539
Inorg. Chem. 2026, 65, 7451−7458

Rietveld method using the $Im\bar{3}$ structural model. The refined structural parameters are presented in Table 1. The lattice

Table 1. Structure Parameters of $LaHg_3Mn_4O_{12}$ with the Space Group $Im\bar{3}$ Refined from the SXRD Pattern at 300 K[a]

parameter	value
a (Å)	7.5949(2)
V (Å^3)	438.103(2)
Z	2
O_y	0.265(1)
O_z	0.207(1)
U_{iso} for La (× 100 Å^2)	0.94(7)
U_{iso} for Hg (× 100 Å^2)	1.34(2)
U_{iso} for Mn (× 100 Å^2)	0.36(2)
U_{iso} for O (× 100 Å^2)	3.32(3)
d_{La-O} (× 12)	2.56(1)
d_{Hg-O} (×4)	2.38(1)
d_{Hg-O} (× 4)	2.85(4)
d_{Mn-O} (× 6)	1.930(2)
∠Mn−O−Mn (°)	159.5(6)
R_{wp} (%)	9.39
R_p (%)	7.45

[a]Atomic Sites: La 2a (0, 0, 0), Hg 6b (0, 0.5, 0.5), Mn 8c (0.25, 0.25, 0.25), and O 24g (0, y, z).

parameter is 7.5949(2) Å, which is apparently larger than those of $RCu_3Mn_4O_{12}$ (~7.3 Å).[14] Notably, the Mn−O−Mn bond angle of $LaHg_3Mn_4O_{12}$ reaches 159.5°. To the best of our knowledge, this is the largest B−O−B bond angle among all reported $AA'_3B_4O_{12}$ quadruple perovskites. In comparison, $RCu_3Mn_4O_{12}$ series typically display Mn−O−Mn angles of about 141°.[14] Figure 1b shows the evolution of ∠Mn−O−Mn as a function of the average A/A′-site ionic radius for $LaHg_3Mn_4O_{12}$ and $RCu_3Mn_4O_{12}$. One finds that the large Hg^{2+} ions at the A′ site effectively expand the crystal lattice and reduce the MnO_6 octahedral tilting, giving rise to a sharply enhanced Mn−O−Mn bond angle in $LaHg_3Mn_4O_{12}$. Figure 1c shows the schematic crystal structure of $LaHg_3Mn_4O_{12}$. Different from the 4-fold coordination CuO_4 squares observed in $RCu_3Mn_4O_{12}$, the larger-size Hg at the A′ site in $LaHg_3Mn_4O_{12}$ forms an 8-fold coordination unit, as reported in the isostructural compound $PbHg_3Ti_4O_{12}$.[31] The structure of $LaHg_3Mn_4O_{12}$ is thus composed of corner-sharing MnO_6 octahedra interconnected with distorted HgO_8 square-prismatic units.

To determine the valence state of Mn ions, we performed XAS measurements at the Mn-L_3 edge, which is highly sensitive to the valence state and local environment of 3d elements.[32,33] Figure 2 shows the Mn-L_3 edge XAS spectrum of $LaHg_3Mn_4O_{12}$, together with $HgMnO_3$ as a Mn^{4+} reference[23] with octahedral coordination, $LaMnO_3$ as a Mn^{3+} reference[34] with octahedral coordination, and $BiMn_3Cr_4O_{12}$ as a Mn^{3+} reference at the A′ site.[6] The detailed multiplet spectral feature of $LaHg_3Mn_4O_{12}$ spectrum can be well reproduced by the superposition of the $HgMnO_3$ spectrum and $LaMnO_3$ spectrum with a 3:1 ratio, suggesting the presence of an average valence state of $Mn^{3.75+}$, fulfilling the charge balance requirement ($La^{3+}Hg^{2+}{}_3Mn^{3.75+}{}_4O^{2-}{}_{12}$) considering La^{3+} and Hg^{2+}. In addition, the good consistency of our simulation indicates that the Mn ions in $LaHg_3Mn_4O_{12}$ exclusively occupy the B-site with an octahedral environment.

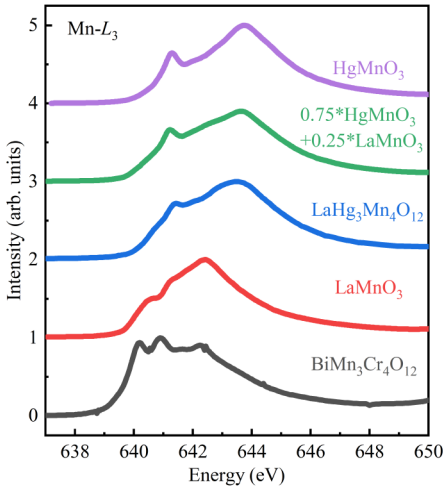

Figure 2. Mn-L_3 XAS spectra of $LaHg_3Mn_4O_{12}$ and of $LaMnO_3$, $HgMnO_3$, and $BiMn_3Cr_4O_{12}$, as presented for references. The green curve stands for the superposition of $HgMnO_3$ and $LaMnO_3$ in a ratio of 3:1.

Figure 3a presents the temperature-dependent magnetic susceptibility of $LaHg_3Mn_4O_{12}$. With decreasing temperature, the susceptibility exhibits a sharp increase at a critical temperature $T_C \approx 280$ K, suggesting the occurrence of a paramagnetic to FM phase transition. Above T_C, e.g., in 300−370 K, the inverse susceptibility can be well fitted using the Curie−Weiss (CW) law with the function $1/\chi = (T - \theta_{CW})/C$ [see the inset of Figure 3a]. The fitting yields the Curie constant C = 10.82 emu·K·mol^{-1}·Oe^{-1} and a Weiss temperature of 281 K, which is consistent with the observed T_C. The effective magnetic moment calculated from the Curie constant is μ_{eff} = 9.30 μ_B/f.u. This value is slightly larger than the theoretical value of 8.30 μ_B/f.u. based on the spin-only model for the average $Mn^{3.75+}$ in $LaHg_3Mn_4O_{12}$. The deviation may originate from dynamic short-range FM correlations present in the paramagnetic phase, as observed in $La_{0.7}Ca_{0.3}MnO_3$ and $(Nd_{1-x}Gd_x)_{0.55}Sr_{0.45}MnO_3$.[35−37]

The field-dependent isothermal magnetization (MH) depicted in Figure 3b shows linear behavior at 350 K, as expected from the paramagnetic state. In comparison, the magnetization curve at 300 K displays an S-shaped feature at lower fields, implying the presence of some short-range FM correlations near T_C. Below T_C, e.g., at 200 and 2 K, canonical FM hysteresis loops are found to occur, in accordance with the long-range FM state. The saturation magnetic moment measured at 2 K is 13 μ_B/f.u., which is in good agreement with the spin-only value expected for an average $Mn^{3.75+}$ valence state. Note that the FM transition can also be identified by a specific heat measurement. As shown Figure 3c, a λ-type anomaly is observed around T_C in the specific heat curve, further confirming the formation of FM ordering in $LaHg_3Mn_4O_{12}$.

Figure 4a shows the temperature-dependent resistivity of $LaHg_3Mn_4O_{12}$ measured at zero field and 8 T. As the temperature decreases, the zero-field resistivity slightly increases, and a dome-like feature forms around T_C. Further cooling leads to a decrease in resistivity below T_C, suggesting the presence of metallic-like electrical transport behavior. Upon the application of an external magnetic field of 8 T, the electrical resistivity is significantly suppressed across the entire temperature range measured. As depicted in Figure 4a, the

https://doi.org/10.1021/acs.inorgchem.6c00539
Inorg. Chem. 2026, 65, 7451−7458

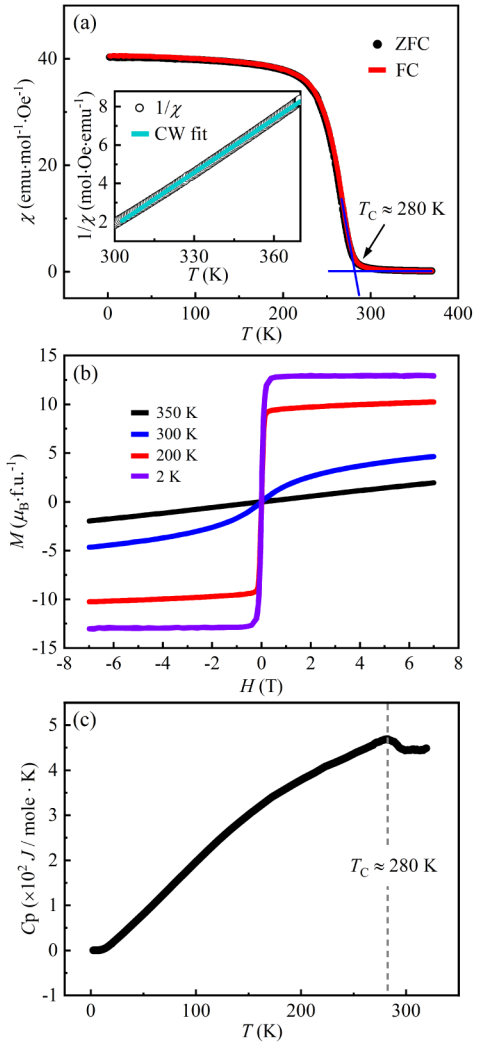

Figure 3. (a) Temperature dependence of the magnetic susceptibility measured at 0.1 T with zero-field-cooling (ZFC) and field-cooling (FC) modes. The blue lines mark the Curie temperature $T_C \approx 280$ K, determined using tangent construction. The inset shows the inverse susceptibility with CW fitting between 300 and 370 K. (b) Field-dependent magnetization (MH) measured at different temperatures. (c) Temperature dependence of the specific heat down to 2 K in zero field.

magnetoresistance (MR), defined as $100\% \times [\rho(H) - \rho(0)]/\rho(0)$, exhibits a kink near T_C, and the absolute value of MR gradually increases with decreasing temperature.

Isothermal field-dependent resistivity measurements were performed to investigate the magnetotransport behavior. As shown in Figure 4b, in the paramagnetic region at 320 K, the resistivity decreases gradually with the applied magnetic field, reaching an MR of −9.2% at 8 T. This is mainly attributed to the suppression of spin fluctuations, where external fields can reduce spin-disorder scattering, promote the hopping of e_g electrons, and thereby increase the conductivity.[38,39] Below T_C, the MR of $LaHg_3Mn_4O_{12}$ displays two distinct features. A remarkably sharp drop in resistivity occurs at lower fields (<1 T). At 2 K, this low-field MR reaches −28.5%, a value that surpasses those observed in the isostructural $RCu_3Mn_4O_{12}$.[13,15,16] In the high-field regime, the MR continues to decrease moderately to a maximum of −38.0% at 2 K and shows no sign of saturation even at the highest

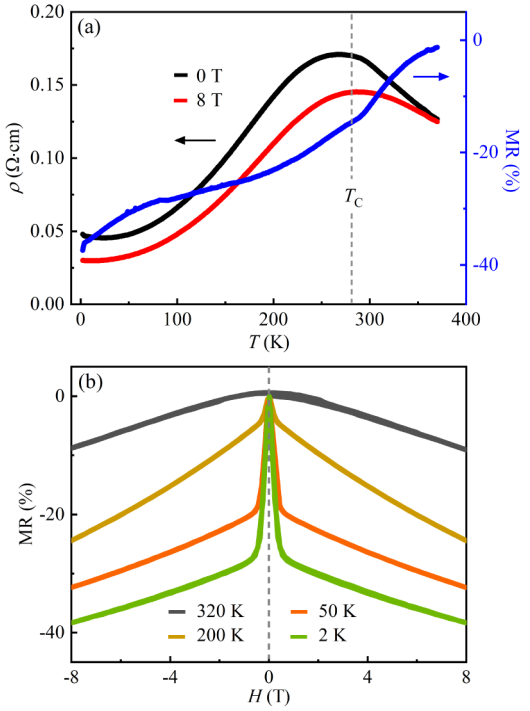

Figure 4. (a) Temperature dependence of resistivity measured at 0 (black) and 8 T (red) for $LaHg_3Mn_4O_{12}$. The blue line shows the temperature-dependent MR curve. (b) Field dependence of MR effects at four selected temperatures.

applied field of 8 T. The pronounced drop in resistivity at low fields can be driven by spin-polarized tunneling across grain boundaries and the alignment of magnetic domains, which facilitates intergrain electron transport.

The magnetic ground state and electronic structure of $LaHg_3Mn_4O_{12}$ were further investigated by spin-polarized first-principles calculations. Three antiferromagnetic (AFM) configurations typical for perovskites (AFM-G, AFM-C, and AFM-A), as well as the FM configuration, were considered to determine the magnetic ground state. As summarized in Table 2, the FM state exhibits the lowest total energy in the entire considered U region, confirming the FM ground state of $LaHg_3Mn_4O_{12}$. To investigate the magnetic properties of the compound in detail, the isotropic exchange interaction parameters J_{ij} were calculated based on the classical Heisenberg model $H = \sum_{i<j} J_{ij}\vec{S}_i\vec{S}_j$ using the Green's function approach

Table 2. Calculated Total Energies of Various Magnetic Configurations and Isotropic Exchange Parameters Obtained within the GGA+U Approximation for Two Hubbard U Values (J_H = 1 eV)[a]

Parameters	U = 3.0 eV	U = 4.5 eV
FM (meV/f.u.)	0	0
AFM-A (meV/f.u.)	80	125
AFM-C (meV/f.u.)	169	258
AFM-G (meV/f.u.)	316	540
J_1 (meV)	−5.2	−11.4
J_2 (meV)	−1.0	−1.5
J_3 (meV)	−0.3	−0.3

[a] J_1, J_2, and J_3 denote the nearest neighbor, next nearest neighbor, and third nearest neighbor exchange interactions, respectively.

https://doi.org/10.1021/acs.inorgchem.6c00539
Inorg. Chem. 2026, 65, 7451−7458

and assuming that spins are unit vectors.[40] The results listed in Table 2 reveal that the nearest-neighbor (J_1), next-nearest-neighbor (J_2), and third-nearest-neighbor (J_3) interactions are all FM, as shown in Figure 5a. This robust FM coupling, particularly the dominant J_1, provides strong theoretical support for the near-room-temperature FM phase observed experimentally.

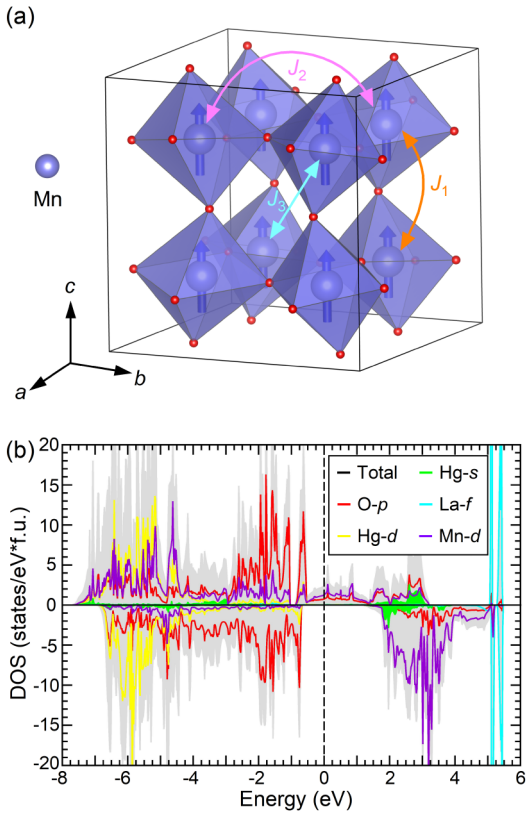

Figure 5. (a) Schematic diagram of the isotropic exchange interaction paths among Mn ions in $LaHg_3Mn_4O_{12}$. The interaction parameters for nearest-neighbor (J_1), next-nearest-neighbor (J_2), and third-nearest-neighbor (J_3) are represented by orange, pink, and cyan colors, respectively. (b) Total and partial density of electronic states (DOS) of $LaHg_3Mn_4O_{12}$ in the FM state obtained in the GGA+U calculations (U = 4.5 eV and J_H = 1.0 eV). The Fermi level is set to 0 eV.

At least several different mechanisms of exchange interactions in $LaHg_3Mn_4O_{12}$ should be considered. First, since the Mn−O−Mn bond angle is rather large, an FM superexchange can occur due to the overlap between half-filled and empty e_g orbitals; this interaction scales as $\sim 1/U$.[41] Additionally, an AFM superexchange between half-filled t_{2g} electrons compensates for this FM term (it is also inversely proportional to Hubbard U). Hopping between e_g orbitals is larger, but there are more channels for the AFM t_{2g}−t_{2g} exchange. The interplay of these terms, the Jahn−Teller effect, and the tendency to change disproportion often result in the so-called CE-type antiferromagnetism as e.g., in such quadruple perovskites as $NaMn_7O_{12}$.[42] $LaHg_3Mn_4O_{12}$ is in a metallic regime in which one can expect a substantial FM double exchange instead, with Mn e_g electrons acting as itinerant carriers and t_{2g} electrons providing localized spins. Finally, an FM indirect exchange interaction via Hg-s states was shown to be essential for explaining the magnetic properties of $HgMnO_3$.[30] Both double and indirect exchange are, to a first approximation, independent of Hubbard U. One can clearly see from Table 2 that the total exchange interaction decreases with U. This is because on-site correlation effects suppress the AFM superexchange, leaving the double and indirect exchanges nearly intact.

Figure 5b displays the density of states (DOS) calculated for the FM ground state. A distinct half-metallic electronic structure is observed: the minority-spin channel exhibits a substantial energy band gap of approximately 2.0 eV, whereas the Fermi level (E_F) crosses the majority-spin bands, resulting in metallic behavior. The conducting majority-spin states primarily have strongly hybridized Mn-3d and O-2p character.[43,44] Such a wide band gap in the insulating channel is crucial for spintronic applications, as it effectively suppresses thermally activated spin-flip transitions, thereby preserving high spin polarization.[45]

Compared to the isostructural $RCu_3Mn_4O_{12}$ family,[13−16] the enhanced half-metallic performance of $LaHg_3Mn_4O_{12}$ can be primarily attributed to the unique role of the nonmagnetic A′ site Hg^{2+} ions and their modulation of the electronic band structure. In $RCu_3Mn_4O_{12}$, the AFM coupling between the magnetic Cu^{2+} at the A′ site and $Mn^{3.75+}$ at the B site leads to a ferrimagnetic order with a reduced net moment. In contrast, the introduction of nonmagnetic Hg^{2+} in $LaHg_3Mn_4O_{12}$ allows the FM moment of the Mn sublattice to be fully released, achieving a large saturation magnetization as high as 13.0 μ_B/f.u., which is approximately 40% higher than that of $RCu_3Mn_4O_{12}$ (~9 μ_B/f.u.). In addition, the introduction of large-sized Hg^{2+} ions significantly expands the lattice and increases the Mn−O−Mn bond angle to 159.5°, which is considerably larger than those observed in $RCu_3Mn_4O_{12}$ (~140°). The reduction of MnO_6 octahedral tilting favors p-d orbital overlap as well as double-exchange interaction. Moreover, the elimination of the Cu^{2+} contribution near the Fermi level leads to strong localization of spin-up electrons and a widening of the minority-spin gap up to ~2.0 eV, which is approximately 600% larger than the ~0.3 eV gap reported in $RCu_3Mn_4O_{12}$.[15,17,18] Note that the nonmagnetic substitution of Cu^{2+} by Hg^{2+} reduces the Curie temperature from ~360 K in $RCu_3Mn_4O_{12}$ to 280 K in the current $LaHg_3Mn_4O_{12}$, suggesting that the $Cu^{2+}(\uparrow)Mn3.75+(\downarrow)$ ferrimagnetic coupling in the former is somewhat stronger than the FM double-exchange interaction in the latter.

4. CONCLUSIONS

In summary, a new A-site-ordered quadruple perovskite $LaHg_3Mn_4O_{12}$ was successfully synthesized at 15 GPa and 1373 K. Synchrotron X-ray diffraction and SAED results confirmed that the compound crystallizes in the cubic $Im\bar{3}$ space group. XAS measurements determined the charge combination to be $LaHg_3Mn^{3.75+}{}_4O_{12}$. An FM phase transition was observed at $T_C \approx 280$ K, accompanied by an electrical transition. Notably, unlike the isostructural $RCu_3Mn_4O_{12}$ compounds, where A′-site magnetic Cu^{2+} ions induce ferrimagnetic coupling with reduced moments, the introduction of nonmagnetic Hg^{2+} in $LaHg_3Mn_4O_{12}$ eliminates the AFM coupling. As a result, a large saturation magnetization of 13.0 μ_B/f.u. is achieved. First-principles calculations indicate that $LaHg_3Mn_4O_{12}$ exhibits a half-metallic electronic structure with a remarkably wide minority-spin energy gap of about 2.0 eV. The combination of high saturation magnetization and a

https://doi.org/10.1021/acs.inorgchem.6c00539
Inorg. Chem. 2026, 65, 7451−7458

wide half-metallic gap makes $LaHg_3Mn_4O_{12}$ a promising material for potential applications in spintronic devices.

AUTHOR INFORMATION

Corresponding Authors

Maocai Pi − *Beijing National Laboratory for Condensed Matter Physics, Institute of Physics, Chinese Academy of Sciences, Beijing 100190, China; School of Physical Sciences, University of Chinese Academy of Sciences, Beijing 100049, China;* orcid.org/0009-0003-2385-0809; Email: pimaocai@iphy.ac.cn

Sergey V. Streltsov − *M. N. Mikheev Institute of Metal Physics UB RAS, Ekaterinburg 620137, Russia*; Email: streltsov.s@gmail.com

Youwen Long − *Beijing National Laboratory for Condensed Matter Physics, Institute of Physics, Chinese Academy of Sciences, Beijing 100190, China; School of Physical Sciences, University of Chinese Academy of Sciences, Beijing 100049, China;* orcid.org/0000-0002-8587-7818; Email: ywlong@iphy.ac.cn

Authors

Ilya Semenov − *Department of Theoretical Physics and Applied Mathematics, Ural Federal University, Ekaterinburg 620002, Russia*

Evgenia Komleva − *M. N. Mikheev Institute of Metal Physics UB RAS, Ekaterinburg 620137, Russia*

Xi Shen − *Beijing National Laboratory for Condensed Matter Physics, Institute of Physics, Chinese Academy of Sciences, Beijing 100190, China*

Huifen Ren − *Synergetic Extreme Condition User Facility (SECUF), Institute of Physics, Chinese Academy of Sciences, Beijing 101400, China*

Zhehong Liu − *Beijing National Laboratory for Condensed Matter Physics, Institute of Physics, Chinese Academy of Sciences, Beijing 100190, China; School of Physical Sciences, University of Chinese Academy of Sciences, Beijing 100049, China;* orcid.org/0000-0001-6731-6040

Jie Zhang − *Beijing National Laboratory for Condensed Matter Physics, Institute of Physics, Chinese Academy of Sciences, Beijing 100190, China; School of Physical Sciences, University of Chinese Academy of Sciences, Beijing 100049, China;* orcid.org/0009-0006-9055-2969

Shuai Tang − *Beijing National Laboratory for Condensed Matter Physics, Institute of Physics, Chinese Academy of Sciences, Beijing 100190, China; School of Physical Sciences, University of Chinese Academy of Sciences, Beijing 100049, China;* orcid.org/0009-0008-5092-067X

Xubin Ye − *Beijing National Laboratory for Condensed Matter Physics, Institute of Physics, Chinese Academy of Sciences, Beijing 100190, China;* orcid.org/0000-0002-5739-8318

Zhiwei Hu − *Max Planck Institute for Chemical Physics of Solids, Dresden 01187, Germany;* orcid.org/0000-0003-0324-2227

Chang-Yang Kuo − *National Synchrotron Radiation Research Center, Hsinchu 30010, Taiwan; Department of Electrophysics, National Yang Ming Chiao Tung University, Hsinchu 30010, Taiwan;* orcid.org/0000-0003-1968-8020

Chien-Te Chen − *National Synchrotron Radiation Research Center, Hsinchu 30010, Taiwan*

Zhao Pan − *Beijing National Laboratory for Condensed Matter Physics, Institute of Physics, Chinese Academy of Sciences, Beijing 100190, China; School of Physical Sciences, University of Chinese Academy of Sciences, Beijing 100049, China;* orcid.org/0000-0002-8693-2508

Yao Shen − *Beijing National Laboratory for Condensed Matter Physics, Institute of Physics, Chinese Academy of Sciences, Beijing 100190, China; School of Physical Sciences, University of Chinese Academy of Sciences, Beijing 100049, China;* orcid.org/0000-0003-4697-4719

Richeng Yu − *Beijing National Laboratory for Condensed Matter Physics, Institute of Physics, Chinese Academy of Sciences, Beijing 100190, China; School of Physical Sciences, University of Chinese Academy of Sciences, Beijing 100049, China;* orcid.org/0000-0002-8086-0910

Complete contact information is available at: https://pubs.acs.org/10.1021/acs.inorgchem.6c00539

Notes

The authors declare no competing financial interest.

ACKNOWLEDGMENTS

This work was supported by the National Key R&D Program of China (Grant No. 2021YFA1400300), the National Natural Science Foundation of China (Grant Nos. 12425403, 12261131499, 12304268, 12304159), and the China Postdoctoral Science Foundation (Grant No. 2023M743741). The synchrotron X-ray powder diffraction experiments were performed at SPring-8 with the approval of the Japan Synchrotron Radiation Research Institute (2024A1506, 2024A1695, and 2025A1495). This work was supported by the Synergetic Extreme Condition User Facility (SECUF, https://cstr.cn/31123.02.SECUF). We acknowledge support from the Max Planck-POSTECH-Hsinchu Center for Complex Phase Materials. The first-principles calculations were supported by the Russian Science Foundation, Russia, via project RSF 23-42-00069. The theoretical analysis was performed within the framework of the state assignment of the Ministry of Science and Higher Education of the Russian Federation for the IMP UB RAS.

REFERENCES

(1) Adams, T. B.; Sinclair, D. C.; West, A. R. Giant barrier layer capacitance effects in $CaCu_3Ti_4O_{12}$ ceramics. *Adv. Mater.* **2002**, *14* (18), 1321−1323.

(2) Ahmadipour, M.; Ain, M. F.; Ahmad, Z. A. A short review on copper calcium titanate (CCTO) electroceramic: synthesis, dielectric properties, film deposition, and sensing application. *Nano Micro Lett.* **2016**, *8* (4), 291−311.

(3) Subramanian, M. A.; Li, D.; Duan, N.; Reisner, B. A.; Sleight, A. W. High Dielectric Constant in $ACu_3Ti_4O_{12}$ and $ACu_3Ti_3FeO_{12}$ Phases. *J. Solid State Chem.* **2000**, *151* (2), 323−325.

(4) Liu, G.; Pi, M.; Zhou, L.; Liu, Z.; Shen, X.; Ye, X.; Qin, S.; Mi, X.; Chen, X.; Zhao, L.; et al. Physical realization of topological Roman surface by spin-induced ferroelectric polarization in cubic lattice. *Nat. Commun.* **2022**, *13* (1), 2373.

(5) Wang, X.; Chai, Y.; Zhou, L.; Cao, H.; Cruz, C.-D.; Yang, J.; Dai, J.; Yin, Y.; Yuan, Z.; Zhang, S.; Yu, R.; Azuma, M.; Shimakawa, Y.; Zhang, H.; Dong, S.; Sun, Y.; Jin, C.; Long, Y. Observation of Magnetoelectric Multiferroicity in a Cubic Perovskite System: $LaMn_3Cr_4O_{12}$. *Phys. Rev. Lett.* **2015**, *115* (8), 087601.

(6) Zhou, L.; Dai, J.; Chai, Y.; Zhang, H.; Dong, S.; Cao, H.; Calder, S.; Yin, Y.; Wang, X.; Shen, X.; et al. Realization of large electric

polarization and strong magnetoelectric coupling in $BiMn_3Cr_4O_{12}$. *Adv. Mater.* **2017**, *29* (44), 1703435.
(7) Kobayashi, W.; Terasaki, I.; Takeya, J.-I.; Tsukada, I.; Ando, Y. A novel heavy-fermion state in $CaCu_3Ru_4O_{12}$. *J. Phys. Soc. Jpn.* **2004**, *73* (9), 2373−2376.
(8) Tanaka, S.; Shimazui, N.; Takatsu, H.; Yonezawa, S.; Maeno, Y. Heavy-mass behavior of ordered perovskites $ACu_3Ru_4O_{12}$ (A = Na, Ca, La). *J. Phys. Soc. Jpn.* **2009**, *78* (2), 024706−024706.
(9) Long, Y.; Saito, T.; Tohyama, T.; Oka, K.; Azuma, M.; Shimakawa, Y. Intermetallic Charge Transfer in A-Site-Ordered Double Perovskite $BiCu_3Fe_4O_{12}$. *Inorg. Chem.* **2009**, *48* (17), 8489−8492.
(10) Long, Y. W.; Hayashi, N.; Saito, T.; Azuma, M.; Muranaka, S.; Shimakawa, Y. Temperature-induced A−B intersite charge transfer in an A-site-ordered $LaCu_3Fe_4O_{12}$ perovskite. *Nature* **2009**, *458* (7234), 60−63.
(11) Yamada, I.; Etani, H.; Tsuchida, K.; Marukawa, S.; Hayashi, N.; Kawakami, T.; Mizumaki, M.; Ohgushi, K.; Kusano, Y.; Kim, J.; Tsuji, N.; Takahashi, R.; Nishiyama, N.; Inoue, T.; Irifune, T.; Takano, M. Control of Bond-Strain-Induced Electronic Phase Transitions in Iron Perovskites. *Inorg. Chem.* **2013**, *52* (23), 13751−13761.
(12) Vasil'ev, A. N.; Volkova, O. S. New functional materials $AC_3B_4O_{12}$ (Review). *Low Temp. Phys.* **2007**, *33* (11), 895−914.
(13) Alonso, J.; Sánchez-Benıtez, J.; De Andrés, A.; Martınez-Lope, M.; Casais, M.; Martınez, J. Enhanced magnetoresistance in the complex perovskite $LaCu_3Mn_4O_{12}$. *Appl. Phys. Lett.* **2003**, *83* (13), 2623−2625.
(14) Sánchez-Benítez, J.; Alonso, J. A.; Falcón, H.; Martínez-Lope, M. J.; De Andrés, A.; Fernández-Díaz, M. T. Preparation under high pressures and neutron diffraction study of new ferromagnetic $RCu_3Mn_4O_{12}$ (R = Pr, Sm, Eu, Gd, Dy, Ho, Tm, Yb) perovskites. *J. Phys.: Condens. Matter.* **2005**, *17* (40), S3063.
(15) Takata, K.; Yamada, I.; Azuma, M.; Takano, M.; Shimakawa, Y. Magnetoresistance and electronic structure of the half-metallic ferrimagnet $BiCu_3Mn_4O_{12}$. *Phys. Rev. B* **2007**, *76* (2), 024429.
(16) Sanchez-Benitez, J.; Alonso, J. A.; Martínez-Lope, M. J.; de Andres, A.; Fernández-Díaz, M. T. Enhancement of the Curie temperature along the perovskite series R $Cu_3Mn_4O_{12}$ driven by chemical pressure of R^{3+} cations (R = rare earths). *Inorg. Chem.* **2010**, *49* (12), 5679−5685.
(17) Liu, X.-J.; Xiang, H.-P.; Cai, P.; Hao, X.-F.; Wu, Z.-J.; Meng, J. A first-principles study of the different magnetoresistance mechanisms in $CaCu_3Mn_4O_{12}$ and $LaCu_3Mn_4O_{12}$. *J. Mater. Chem.* **2006**, *16* (43), 4243−4248.
(18) Chen, L.; Wang, C. L. First principles study of the electron structures of $CaCu_3Mn_4O_{12}$ and $CaCu_3Ti_4O_{12}$. *J. Magn. Magn. Mater.* **2007**, *312* (2), 266−270.
(19) Sánchez-Benítez, J.; Alonso, J. A.; de Andrés, A.; Martínez-Lope, M. J.; Martínez, J. L.; Muñoz, A. Peculiar Magnetic Behavior of the $TbCu_3Mn_4O_{12}$ Complex Perovskite. *Chem. Mater.* **2005**, *17* (20), 5070−5076.
(20) Sánchez-Benítez, J.; Martínez-Lope, M. J.; Alonso, J. A. Preparation at moderate pressures, crystal and magnetic structure and magnetotransport of the ferrimagnetic $CeCu_3Mn_4O_{12}$ perovskite. *J. Appl. Phys.* **2010**, *107* (10), 103904.
(21) Kanamori, J. Superexchange interaction and symmetry properties of electron orbitals. *J. Phys. Chem. Solids* **1959**, *10* (2−3), 87−98.
(22) Zhou, J.; McDevitt, J.; Zhou, J.; Yin, H.; Goodenough, J.; Gim, Y.; Jia, Q. Effect of tolerance factor and local distortion on magnetic properties of the perovskite manganites. *Appl. Phys. Lett.* **1999**, *75* (8), 1146−1148.
(23) Zhou, B.; Qin, S.; Ma, T.; Ye, X.; Guo, J.; Yu, X.; Lin, H.-J.; Chen, C.-T.; Hu, Z.; Tjeng, L.-H.; Zhou, G.; Dong, C.; Long, Y. High-Pressure Synthesis of Two Polymorphic $HgMnO_3$ Phases and Distinct Magnetism from 2D to 3D. *Inorg. Chem.* **2020**, *59* (6), 3887−3893.
(24) Zhou, B. W.; Zhang, J.; Ye, X. B.; Liu, G. X.; Xu, X.; Wang, J.; Liu, Z. H.; Zhou, L.; Liao, Z. Y.; Yao, H. B.; Xu, S.; Shi, J. J.; Shen, X.; Yu, X. H.; Hu, Z. W.; Lin, H. J.; Chen, C. T.; Qiu, X. G.; Dong, C.; Zhang, J. X.; Yu, R. C.; Yu, P.; Jin, K. J.; Meng, Q. B.; Long, Y. W. Octahedral Distortion and Displacement-Type Ferroelectricity with Switchable Photovoltaic Effect in a $3d^3$-Electron Perovskite System. *Phys. Rev. Lett.* **2023**, *130* (14), 146101.
(25) Zhang, J.; Ye, X.; Wang, X.; Pan, Z.; Pi, M.; Tang, S.; Dong, C.; Chen, C.-T.; Chen, J.-M.; Kuo, C.-Y.; Hu, Z.; Shen, X.; Yu, X.; Shen, Y.; Yu, R.; Long, Y. Realization of Intrinsic Colossal Magnetoresistance in $Pb(Pb_{1/3}Hg_{2/3})_3Mn_4O_{12}$: An A Site-Ordered Quadruple Perovskite Oxide. *J. Am. Chem. Soc.* **2025**, *147* (15), 12644−12651.
(26) Toby, B. EXPGUI, a graphical user interface for GSAS. *J. Appl. Crystallogr.* **2001**, *34* (2), 210−213.
(27) Kresse, G.; Furthmüller, J. Efficient iterative schemes for ab initio total-energy calculations using a plane-wave basis set. *Phys. Rev. B* **1996**, *54* (16), 11169−11186.
(28) Liechtenstein, A. I.; Katsnelson, M.; Antropov, V.; Gubanov, V. Local spin density functional approach to the theory of exchange interactions in ferromagnetic metals and alloys. *J. Magn. Magn. Mater.* **1987**, *67* (1), 65−74.
(29) Perdew, J. P.; Burke, K.; Ernzerhof, M. Generalized Gradient Approximation Made Simple. *Phys. Rev. Lett.* **1997**, *78* (7), 1396−1396.
(30) Myakotnikov, D. A.; Komleva, E. V.; Long, Y.; Streltsov, S. V. Importance of the indirect exchange interaction via s states in altermagnetic $HgMnO_3$. *Phys. Rev. B* **2024**, *110* (13), 134427.
(31) Zhao, J.; Gao, J.; Li, W.; Qian, Y.; Shen, X.; Wang, X.; Shen, X.; Hu, Z.; Dong, C.; Huang, Q.; et al. A combinatory ferroelectric compound bridging simple ABO_3 and A-site-ordered quadruple perovskite. *Nat. Commun.* **2021**, *12* (1), 747.
(32) Burnus, T.; Hu, Z.; Wu, H.; Cezar, J. C.; Niitaka, S.; Takagi, H.; Chang, C. F.; Brookes, N. B.; Lin, H.-J.; Jang, L. Y.; et al. X-ray absorption and x-ray magnetic dichroism study on Ca_3CoRhO_6 and Ca_3FeRhO_6. *Phys. Rev. B* **2008**, *77* (20), 205111.
(33) Hollmann, N.; Valldor, M.; Wu, H.; Hu, Z.; Qureshi, N.; Willers, T.; Chin, Y.-Y.; Cezar, J. C.; Tanaka, A.; Brookes, N. B.; et al. Orbital occupation and magnetism of tetrahedrally coordinated iron in $CaBaFe_4O_7$. *Phys. Rev. B* **2011**, *83* (18), 180405.
(34) Burnus, T.; Hu, Z.; Hsieh, H. H.; Joly, V. L. J.; Joy, P. A.; Haverkort, M. W.; Wu, H.; Tanaka, A.; Lin, H. J.; Chen, C. T.; Tjeng, L. H. Local electronic structure and magnetic properties of $LaMn_{0.5}Co_{0.5}O_3$ studied by x-ray absorption and magnetic circular dichroism spectroscopy. *Phys. Rev. B* **2008**, *77* (12), 125124.
(35) Dai, P.; Fernandez-Baca, J. A.; Wakabayashi, N.; Plummer, E. W.; Tomioka, Y.; Tokura, Y. Short-Range Polaron Correlations in the Ferromagnetic $La_{1-x}Ca_xMnO_3$. *Phys. Rev. Lett.* **2000**, *85* (12), 2553−2556.
(36) Souza, J. A.; Neumeier, J. J.; Yu, Y.-K. Magnetic signatures of ferromagnetic polarons in $La_{0.7}Ca_{0.3}MnO_3$: Colossal magnetoresistance is not a Griffiths singularity. *Phys. Rev. B* **2008**, *78* (1), 014436.
(37) Kamel, R.; Tozri, A.; Dhahri, E.; Hlil, E. K. Anomalous behavior above the Curie temperature in $(Nd_{1-x}Gd_x)_{0.55}Sr_{0.45}MnO_3$ (x = 0, 0.1, 0.3 and 0.5). *RSC Adv.* **2019**, *9* (47), 27541−27548.
(38) Haas, C. Spin-Disorder Scattering and Magnetoresistance of Magnetic Semiconductors. *Phys. Rev.* **1968**, *168* (2), 531−538.
(39) von Helmolt, R.; Wecker, J.; Holzapfel, B.; Schultz, L.; Samwer, K. Giant negative magnetoresistance in perovskitelike $La_{2/3}Ba_{1/3}MnO_x$ ferromagnetic films. *Phys. Rev. Lett.* **1993**, *71* (14), 2331−2333.
(40) Korotin, D. M.; Mazurenko, V.; Anisimov, V.; Streltsov, S. Calculation of exchange constants of the Heisenberg model in plane-wave-based methods using the Green's function approach. *Phys. Rev. B* **2015**, *91* (22), 224405.
(41) Streltsov, S. V.; Khomskii, D. I. Orbital physics in transition metal compounds: new trends. *Phys.-Usp.* **2017**, *60* (11), 1121.
(42) Streltsov, S. V.; Khomskii, D. I. Jahn-Teller distortion and charge, orbital, and magnetic order in $NaMn_7O_{12}$. *Phys. Rev. B* **2014**, *89* (20), 201115.
(43) Anderson, P. W.; Hasegawa, H. Considerations on Double Exchange. *Phys. Rev.* **1955**, *100* (2), 675−681.

https://doi.org/10.1021/acs.inorgchem.6c00539
Inorg. Chem. 2026, 65, 7451−7458

(44) Park, J. H.; Vescovo, E.; Kim, H. J.; Kwon, C.; Ramesh, R.; Venkatesan, T. Direct evidence for a half-metallic ferromagnet. *Nature* **1998**, *392* (6678), 794−796.
(45) Katsnelson, M. I.; Irkhin, V. Y.; Chioncel, L.; Lichtenstein, A. I.; de Groot, R. A. Half-metallic ferromagnets: From band structure to many-body effects. *Rev. Mod. Phys.* **2008**, *80* (2), 315−378.

https://doi.org/10.1021/acs.inorgchem.6c00539
Inorg. Chem. 2026, 65, 7451−7458